Journal of Materials Chemistry A

# Unprecedented $CO_2$ adsorption behaviour by 5A-type zeolite discovered in lower pressure region and at 300 K



| | |
|---|---|
| Journal: | *Journal of Materials Chemistry A* |
| Manuscript ID | TA-ART-10-2020-009944.R2 |
| Article Type: | Paper |
| Date Submitted by the Author: | 02-Feb-2021 |
| Complete List of Authors: | Oda, Akira; Okayama University, Department of Materials Chemistry<br>Draduate School of Engineering Nagoya University<br>Hiraki, Suguru; Okayama University<br>Harada, Eiji; Okayama University<br>Kobayashi, Ikuka; Okayama University<br>Ohkubo, Takahiro; Okayama University, Department of Chemistry<br>Ikemoto, Yuka; JASRI/SPring-8, Spectroscopy and Imaging Devision<br>Moriwaki, Taro; JASRI/SPring-8,<br>Kuroda, Yasushige; Okayama Daigaku, Department of Chemistry |
| | |

# Unprecedented $CO_2$ adsorption behaviour by 5A-type zeolite discovered in lower pressure region and at 300 K

Akira Oda,[1] Suguru Hiraki,[1] Eiji Harada,[1] Ikuka Kobayashi,[1] Takahiro Ohkubo,[1] Yuka Ikemoto,[2] Taro Moriwaki[2] and Yasushige Kuroda*[1]

[1]Department of Chemistry, Graduate School of Natural Science and Technology, Okayama University, 3-1-1 Tsushima-naka, Kita-ku, Okayama 700-8530, Japan.

[2]Japan Synchrotron Radiation Research Institute (JASRI), 1-1-1, Kouto, Sayo-cho, Sayo-gun, Hyogo 679-5198, Japan.

***Corresponding author e-mail:** kuroda@cc.okayama-u.ac.jp

Mitigation of the amounts of $CO_2$ in the environment is one of the most urgent problems requiring a solution. To fulfil this demand, efficient adsorbents for $CO_2$ are required that work at room temperature (RT) and in a lower pressure region of not more than 5000 ppm under the ambient condition. In the present work, specific and selective adsorption of $CO_2$ onto NaCaA-85 (A-type zeolite with an ion-exchange capacity of 85%) was observed at the required conditions; the amounts of adsorbed $CO_2$ on the NaCaA-85 sample were far larger than amounts reported for other materials in the pressure range from 400 to 5000 ppm. The characteristic adsorption mechanism induced by this material was verified directly through methods combining synchrotron-based far-infrared (far-IR) measurements with a computational technique. The resultant $Ca^{2+}$-framework vibration modes for the NaCaA-85 sample were observed at 266 and 246 $cm^{-1}$, which shifted toward the lower wave-numbers, i.e., 225 and 203 $cm^{-1}$, after $CO_2$ adsorption at RT, respectively. The observed characteristic property was explained by a model consisting of a $CO_2$ molecule simultaneously pinned by two $Ca^{2+}$ ions positioned on two types of exchangeable sites composed of 8- and 6-membered rings, which was well supported with the density functional theory calculation method. This characteristically adsorbed $CO_2$ species was completely desorbed, and the original state easily recovered through evacuation around 400 K. In addition, the selective adsorption behaviour of $CO_2$ from other gases, such as $H_2$, $CH_4$, $O_2$ and $N_2$, was found at RT. On the basis of these data, the separation property of $CO_2$ were examined by measuring the breakthrough curve using the model gas composed of 0.04% $CO_2$, 20% $O_2$ and 79.96% $N_2$, which mimicked ambient air, indicating the superior separation feature. These findings may pave a new way for the use of the NaCaA-85 material as an efficient adsorbent for selective $CO_2$ adsorption functioning at RT and in the lower pressure region of up to 5000 ppm.

## Introduction

Climate change has become a major issue in the world, and there is at present a general consensus that it is due to the emission of greenhouse gases (GHGs), in particular, $CO_2$, resulting from anthropogenic activities. The World Meteorological Organization reported in 2019 that the mean concentration of $CO_2$ in the atmosphere on Earth has surpassed 400 ppm:[1] it increased from 405.5 (in 2017) to 407.8 ppm (in 2018), and has increased by *ca.* 130 ppm overall since the start of the Industrial Revolution (*ca.* 280 ppm).[2] The combustion of fossil fuels as energy sources and also their transformation to value-added products are largely responsible for this increase, yet even in the 21st century, fossil fuels will continue to be used more or less as a source of energy and for producing chemical materials as a complete consensus regarding the reduction of their discharge level has not been reached even at the United Nations Climate Change Conference held in Chile in 2019 (COP25). In addition, $CO_2$ thus released is thermodynamically very stable and is a kinetically inert material in the general condition with the exception of the strong alkaline condition; however, $CO_2$ captured in alkaline materials obstructs reuse for the chemical starting material, although the conversion of $CO_2$ into useful materials has also been an essential target derived from carbon capture procedures.[3,4]

Under these circumstances, the development of a method for the separation of GHGs from dilute emissions was proposed by Sholl and Lively as one of "seven chemical separations to change the world".[5] In this era, we must therefore search for methods to capture $CO_2$ selectively under ambient conditions.[6,7] One effective way of mitigating $CO_2$ emission is to eliminate it directly from flue gases in power plants and natural gas[8–12] by using materials with a strong alkaline nature, such as amine, NaOH, soda lime, etc.[13–17] In relation to these processes, the removal of $CO_2$ is dominantly focused on the higher pressure region of $CO_2$, where various methods have been successful. In addition, from the viewpoint of direct separation of $CO_2$ with higher concentration from other gases, pressure swing adsorption and temperature swing adsorption might be additional useful methods that use solid materials.[18–21] By contrast, there is renewed interest in the possibility of $CO_2$ storage and separation procedures in the lower pressure regime, from 0 to 5000 ppm,[22,23] where 5000 ppm is the recommended exposure limit by the National Institute for Occupational Safety and Health guidelines,[24] although such processes involve many difficulties. Therefore, processes for the separation, storage and transformation of $CO_2$ are urgently required to establish the easy use of recovered $CO_2$ with higher purity, targeting its lower concentration level for converting into valuable chemicals. One possible separation process is referred to as direct air capture (DAC), which is another area of study for $CO_2$ capture under atmospheric conditions: the concentration of *ca.* 400 ppm in 1 bar atmosphere at 300 K. In such a case, it is necessary to develop materials that have efficient adsorption for $CO_2$ removal and that simultaneously permit easy desorption, thus aiming at reusing these materials for

potential application under DAC conditions.[25–30] Therefore, the development of high-performance materials with outstanding adsorption capacity under the lower pressure condition is one of the new great challenges for chemists. Amine-functionalized porous oxides, polymers, and metal-organic frameworks (MOFs), as well as ionic liquid materials, are now attracting increasing interest.[14,30–40] In particular, MOFs with 4,4′-dioxidobiphenyl-3,3′-dicarboxylate ($dobpdc^{4-}$)[35,37] or biphenyl-3,3',5,5'-tetracarboxylate ($bptc^{4-}$)[38] modified with amine groups are experiencing a renaissance because of their singular adsorbability in the lower pressure region. Over the past several years, a considerable number of studies have dealt with the development of efficient MOF materials having excellent $CO_2$ adsorption.[41–49] However, major materials that exhibit excellent $CO_2$ adsorption have an amine group as a basic site, i.e., the idea adopted is normal and will have a tendency to degrade or corrode the composites. In addition, the strong alkaline condition is not suitable for recycling the adsorbates. Among these studies, materials mimicking the enzymatic model incorporated as a chemical part are attractive for $CO_2$ adsorbents: nucleophilic hydroxyl binding sites (biomimetic Zn–OH species).[50–54] By contrast, it is generally accepted that zeolites (a type of aluminosilicates) without special surface modification have no specific adsorption for $CO_2$ around room temperature (RT), in particular in the lower pressure region, because they have no effective sites for $CO_2$ at RT, such as strong basic sites that are expected to be operative as active sites for a $CO_2$ molecule with acidic nature. Zeolites are better known as materials used in the high pressure regions.[18–20] Therefore, less attention has been paid to zeolite materials as adsorbents working in DAC conditions. Because of the low adsorption capacity of $CO_2$ and the poor selectivity over $N_2$ in the lower pressure adsorption region, zeolites have not yet been recognized as good materials for $CO_2$ capture functioning in the lower pressure regions.[55–58] In practice, surprisingly, to date few studies on zeolite have focused on $CO_2$ adsorption behaviour at RT in the lower pressure region: Figure SI-1.[59] In these circumstances, the design of efficient adsorbents for $CO_2$ storage based on abundant and stable metal ions, such as alkali-metal and alkaline-earth-metal ions, together with aluminosilicates for widespread use in the DAC process, is a prominent challenge. The design of efficient adsorbents for $CO_2$ storage based on abundant materials is therefore essential for increasing the adsorption capacities at extremely low $CO_2$ concentrations ranging from 400 to 5000 ppm and at RT.[60–62]

Here, we designed an ion-exchanging method of zeolite with alkaline-earth ions and succeeded in achieving outstanding adsorption of $CO_2$ in the lower pressure region from 400 to 5000 ppm at RT onto a $Ca^{2+}$-ion-exchanged A-type zeolite and aimed at clarifying its specificity against the $CO_2$ molecule. As a result, this specificity was caused by two kinds of $Ca^{2+}$-ions exchanged in A-type zeolite with appropriate curvature created by pore-wall which bring into positions favourable to stable and selective trapping of $CO_2$. It will be applicable also to cleaning air in semi-closed spaces, such as a space shuttle, a submarine, or a concert hall, and would also

be useful for a $CO_2$-adsorbent material accessible for anaesthetic purposes.[63,64]

## Results and discussion

### (I) Outstanding $CO_2$ adsorption of the NaCaA-85 sample observed at RT and in the lower pressure region

#### (a) Adsorption behaviour

The A-type zeolite with a Si/Al ratio of 1 was selected for this work, because it enabled more adsorption sites, and it had an appropriate pore size for the adsorbate, i.e., the $CO_2$ molecule. In addition, alkaline-earth ion-exchanged A-type zeolites seem to be suitable for $CO_2$ adsorption because of their larger electric field strength, which may be expected to work as an important driving force for the adsorption behaviour for the $CO_2$ molecule in the lower pressure region. The latter consideration is shown clearly in Figure 1. The Na ion has the same ionic radius as the divalent Ca ion; the adsorbed amount of the original NaA sample is far smaller than that observed for the NaCaA-85 sample, in particular in the lower pressure region. By contrast, the sample exchanged with the divalent ions having a larger ionic radius was not suitable as the adsorbent because it may block the insertion of the $CO_2$ molecule into the pore formed by the framework of the A-type zeolite. The A-type zeolite sample exchanged with the $Ba^{2+}$ ion having an ionic radius of 1.35 Å can hardly adsorb the $CO_2$ molecule at RT as given in Figure 1,[65] which is interpreted in terms of the blocking with the $Ba^{2+}$ ion from the invading of $CO_2$ into the pore, although the Ba-ion-exchanged MFI-type zeolite is a very efficient material for $CO_2$ adsorption (see also Figure SI-1).[59] The most important point of note in this figure is the characteristic adsorption feature found in the NaCaA-85 sample. This sample exhibits an outstanding adsorption property for $CO_2$ even at 298 K, especially under the lower pressure of 0.01 Torr, which indicates an adsorbed amount of *ca.* 16.8 $cm^3\ g^{-1}$ (0.75 mmol $g^{-1}$) together with the appearance of a characteristic gentle step in the adsorption isotherm at around 0.004 Torr (Figure 1b). This sample gives an adsorption value of *ca.* 40 $cm^3\ g^{-1}$ (1.8 mmol $g^{-1}$ converting to a ratio of 0.59, $CO_2/Ca^{2+}$) at 0.3 Torr, which corresponds to the partial amount of *ca*. 400 ppm $CO_2$ in ambient air (Figure 1c). To our knowledge, this is the first example found in the zeolite systems to give such an adsorption value and it is situated in the 4$^{th}$ position among various systems reported so far (Figure SI-1).[34,37–39,43,54,59] The adsorbed amount observed at the equilibrium pressure of 3.8 Torr (5000 ppm) yields 72 $cm^3\ g^{-1}$ (3.2 mmol $g^{-1}$) (Figure 1d). Furthermore, the NaCaA-85 sample exhibits a very high adsorption in the 5000 ppm region, compared with the data for Zn-complex systems.[54] To the authors' knowledge, there have been no previous reports on such a high adsorption property for $CO_2$ functioning at RT and in the lower pressure region of 400 to 5000 ppm using a 5A-type zeolite or other materials. This sample also showed the highest adsorption volume even in the higher pressure region of *ca.* 100 Torr among the samples examined in this work (Figure

1a). These adsorption properties are far superior to those observed for the 5A sample reported by National Aeronautics and Space Administration and in similar works.[66–68] Recently, Bae *et al*. reported outstanding adsorption for the 5A sample at a pressure of 1 bar, but the reported condition only focused on the higher pressure region up to 1 bar and the authors do not discuss the specificity observed in the lower pressure region.[69] Our results show higher adsorption, even in the higher pressure region. On the basis of these data, this sample is expected to be the singular candidate adsorbent that would work in DAC conditions. In addition, the Sr-ion-exchanged sample, i.e., NaSrA-71, also seems to be effective for $CO_2$ adsorption, but does not adsorb an amount as large as the case of NaCaA-85.

The second adsorption was performed after evacuation at 298 K of the samples on which the first adsorption measurements were performed. The difference in the amount adsorbed between the first and second adsorption for the NaCaA-85 sample means the existence in the strongly adsorbed species which was not desorbed from this sample even after the evacuation at RT. This difference in NaCaA-85 is largest among the samples used in this work. Judging from the comparison between the first and second adsorption isotherm on NaCaA-85, the strongly adsorbed species formed at around the equilibrium pressure of 0.004 Torr, resulting in the appearance of a gentle step in the first isotherm that was completely lost in the second adsorption process: Figure 1b.

In the following stage, we intended to examine the specificity of the Ca-ion-exchanged A-type zeolite, i.e., the NaCaA-85 sample, which works as an excellent adsorbent for the $CO_2$ molecule under lower pressure and at RT even in the case that it has no characteristic basic sites for a $CO_2$ molecule with an acidic nature. For comparison, we used two kinds of samples with lower exchanging levels: the purchased sample from Sigma-Aldrich Co., i.e., the CaA-78 sample, and the NaCaA–65 sample with a lower exchange level; the latter sample was ion exchanged in our laboratory with NaA. The adsorbed amounts of the former sample were 12 $cm^3\ g^{-1}$ and for the latter sample 28 $cm^3\ g^{-1}$, respectively, even at the equilibrium pressure of 0.3 Torr. These amounts are far smaller than the amount for NaCaA-85, i.e., 40 $cm^3\ g^{-1}$ (Figure 2). As expected, the rising tendency found in the lower pressure region around 0.004 Torr was inhibited in both samples with lower exchange capacities (Figure 2b). It is the ion-exchange capacity, in particular the increase in the $Ca^{2+}$ ion amount from 65% or 78% to 85%, that gives rise to the distinct specific feature working in the presence of $CO_2$ around 400 ppm. This specific adsorption feature recognized in the equilibrium pressure range of 0.003 to 0.015 Torr is the prominent feature and is essential for developing the specific $CO_2$ adsorption state shown by the NaCaA-85 sample.

At this stage, we needed to obtain information on the dominant driving force causing the specific $CO_2$ adsorption detected in the NaCaA-85 sample. At first, the detailed comparison of isotherms among Mg-, Ca-, and Sr-ion-exchanged samples excluded the crucial operation based

only on the electric field effect emanating from the charges on the exchanged cations as a dominant contribution (Tables SI-1 and SI-2). Furthermore, the specific adsorption in the lower pressure region was observed mainly in the NaCaA-85 system and not in the CaA-78 and NaCaA-65 samples or in the NaMgA-42 sample, indicating that the $CO_2$ forms specific interaction through some kind of chemical bonding nature that prevails against the electrostatic field. Judging from the data for CO adsorption on the NaCaA-85 sample (Figure SI-2) and also based on the $CO_2$ adsorption behaviour observed for the NaSrA-71 sample, the contribution from the dipole interaction, as well as the polarization of cations, is also precluded (Tables SI-1 and SI-2). These facts indicate the existence of a specialized interaction in the NaCaA-85 sample: the singular bonding formation between a $Ca^{2+}$ ion or ions and $CO_2$.

**(b) Energetic properties**

The heats of adsorption were examined for the energetic features on the respective samples (Figure 3). For the first adsorption of $CO_2$ on the NaCaA-85 sample, a higher heat value of *ca*. 65 kJ $mol^{-1}$ was observed in the initial stage and it decreased steeply to 60 kJ $mol^{-1}$. This indicated the existence of some heterogeneous and active sites on the sample. After this stage, it was clearly seen that the NaCaA-85 sample, which showed a specific adsorption property in the lower pressure region, exhibited a "flat region" showing an adsorption heat of *ca.* 60 kJ $mol^{-1}$: Figure 3a. This flat part corresponded well with the sudden increase in the adsorption isotherm around the pressure of 0.004 Torr (see Figure 1b), indicating that there were some energetically homogeneous sites for $CO_2$ adsorption, which afforded the peculiar $CO_2$ adsorption sites in the lower pressure region. After establishing the adsorption amount of *ca.* 20 $cm^3$ $g^{-1}$, the adsorption heat gradually reduces through an S-shaped curve, and finally reduces to 35.5 kJ $mol^{-1}$ with increasing the adsorbed amount to 118 $cm^3$ $g^{-1}$. In this connection, the differential adsorption heats of $CO_2$ on some zeolite systems have been reported by Azevedo *et al*.[70] and the heat of bcondensation of $CO_2$ was reported by Arrigio *et al*. to be 17 kJ $mol^{-1}$.[71] By contrast, the initial states including the heterogeneous (steeply decreasing part) and homogeneous (flat part) adsorption processes were completely lacking in the second adsorption process, as if the second adsorption heat curve overlapped with the first by shifting the strong adsorption amount of *ca.* 25 $cm^3$ $g^{-1}$ toward a higher adsorption side. On the behaviour of the heat of adsorption on the CaA-78 sample, the initial heat of 60 kJ $mol^{-1}$ was obtained and subsequently a monotonous decrease without a flat part was observed with increasing amounts of $CO_2$ adsorption. In addition, the second adsorption behaviour is almost same as the first one. For the NaCaA-65 sample, the first adsorption heat of 63 kJ $mol^{-1}$ was observed in the initial stage; it decreased to 49 kJ $mol^{-1}$ with increasing adsorption amounts and attained 36 kJ $mol^{-1}$ in the final stage: Figure 3b. In this case, the flat part was also hardly found in the adsorption heat. In the second process, a smaller adsorption heat of 57 kJ $mol^{-1}$ was observed in the lower pressure region. Similar to NaCaA-85,

it seems that the second adsorption heat curve overlapped with the first one by shifting the adsorption amount of *ca.* 15 $cm^3$ $g^{-1}$ toward the higher adsorption side.

At the risk of repeating our statements, we would like to emphasize that these adsorption data on the samples, i.e., both CaA-78 and NaCaA-65, added strong support for the idea that in the lower pressure region the NaCaA-85 sample involves characteristic binding sites for $CO_2$.

**(c) Desorption behaviour**

The temperature programmed desorption (TPD) measurement for the NaCaA-85 sample evacuated at 300 K after treating with $CO_2$ of 100 Torr at 300 K for the sample evacuated at 723 K was allowed to perform until the temperature reached 873 K by using a mass spectrometer as a detector of $m/z = 44$. The observed desorption behaviour of $CO_2$ is shown in Figure 4. One broad desorption band, centred at 400 K (127 ℃), was clearly recognized; this band was resolved into two components centred at 365 K (92 ℃) and at 405 K (132 ℃), respectively, which are depicted by blue (b) and (c) red lines, respectively; these components indicate the existence of at least two kinds of irreversibly-adsorbed species. No bands of the desorbed gas beyond the temperature at 473 K were observed, clearly indicating the lack of carbonate species formation on this sample in this experiment. Taking into account the TPD data, this sample was expected to have reuse feasibility through evacuation at less than 473 K.

**(II) Far-IR and mid-IR studies supported by a DFT study**

**(a) Study on the basis of far-IR spectra**

No effective methods have been presented to date for clarifying the specificity observed in this work. On the basis of the origin of the vibrational modes, the far-IR spectra of the zeolite samples from 600 to 30 $cm^{-1}$ can be roughly divided into two regions, namely the framework vibration mode[72–76] above *ca.* 300 $cm^{-1}$ and the exchanged cation-framework vibrational mode[76–80] below *ca.* 300 $cm^{-1}$. In addition, there is some feasibility caused by the coupling of lattice-vibration modes with cation-motion modes, resulting in analytical difficulty. Fortunately, in the case of A-type zeolite, it is generally known that other bands except the cation-framework vibration modes scarcely appear in the lower wave-number region below 300 $cm^{-1}$. This makes it possible to observe exclusively the change in far-IR spectra due to cation-framework vibration upon adsorption of $CO_2$ at RT. In line with these bases, we examined the IR bands in the far-IR region with the synchrotron radiation source; typical spectra of the NaCaA-85 sample before and after $CO_2$ adsorption at RT in the region from 600 to 100 $cm^{-1}$ are shown in Figure SI-3. The bands with larger intensities observed between 600 and 300 $cm^{-1}$ were assignable to the framework modes: the 555 $cm^{-1}$–band to symmetric stretching vibration, the 466 $cm^{-1}$– and 370 $cm^{-1}$–bands to bending vibrations to 4-membered rings (MRs), as well as 6- or 8-MRs.[73] However, in the range between 600 and 300 $cm^{-1}$, the bands observed behave in a very complex nature

during the $CO_2$ adsorption processes (Figure SI-3).

On the basis of these fundamental viewpoints, we focused on the cation-framework vibrational modes. To the best of our knowledge, to date only a few works examined the adsorption behaviour *in situ* condition through the far-IR method performed for the zeolite samples evacuated at higher temperatures.[81–84] Depicted in Figures 5a–c are the far-IR spectra measured at RT between 350 and 100 $cm^{-1}$ for the NaCaA-85, CaA-78 and NaA samples evacuated at 723 K and subsequently exposed to $CO_2$ at RT under the *in situ* condition, followed by re-evacuation to 423 K. From the spectrum of the NaCaA-85 sample (Figure 5a), there are two dominant types of bands in the range of *ca.* 300–200 $cm^{-1}$, i.e., centred at 266 and 240 $cm^{-1}$, respectively, which are assigned to the cations-framework vibration modes, although the latter band appears as a shoulder of the former band. We could not find other obvious bands in this region except the extremely weak broad bands with a shoulder in the lower wave-number regions. We ensured that the two kinds of distinct bands just mentioned shift toward the lower wave-number side upon $CO_2$ adsorption at RT; the former band decreases in intensity and the shoulder band at 240 $cm^{-1}$ also loses intensity, resulting in a shift toward the lower wave-number side and appearing as new bands at 225 and 203 $cm^{-1}$, respectively (see also the difference spectrum shown in Figure SI-4a). These findings clearly indicated that the cation-framework vibrational modes were affected by the $CO_2$-adsorption. The presence of two kinds of bands even after $CO_2$ adsorption supports that both sites work as the effective $CO_2$ adsorption sites. By contrast, the CaA-78 sample gives similar bands in the region between 300 and 200 $cm^{-1}$, together with a shoulder band around 180 $cm^{-1}$ (Figure 5b), whereas a change in the spectrum is not found as a distinct observation even after the adsorption of $CO_2$ at RT; the slight increase in band-intensity looks like a skirt toward the lower wave-number region. These points can be easily recognized in the difference spectrum (Figure SI-4c). It is a characteristic feature that the CaA-78 sample did not show any distinctive changes in the spectrum even after $CO_2$ adsorption at RT. For the case of NaA, there were hardly any changes in the spectrum after $CO_2$ adsorption (Figure 5c). Taking these results into consideration, the far-IR spectra of NaCaA-85 before and after $CO_2$ adsorption present quite characteristic features in comparison with CaA-78 and NaA. Furthermore, with the desorption behaviour (Figure 4) and with the difference observed between the first and second adsorption data for the NaCaA-85 sample (Figures 1 and 3) in mind, the spectrum of the NaCaA-85 sample on which $CO_2$ was adsorbed was also measured after evacuating the sample with adsorbed $CO_2$ at 300 K for 30 min (Figure 5a: the spectrum depicted by blue line). There are only small changes after this treatment; the spectrum has quite a similar pattern to the spectrum depicted by the red line (Figure 5a) measured in the presence of $CO_2$ in the gas phase, indicating that the feature observed in the spectra was practically caused by the "irreversibly adsorbed $CO_2$ species" formed on this sample (Figure SI-4b). These species were completely desorbed after

evacuating at 423 K and the spectrum recovered to the original for the sample evacuated at 723 K (the green line and also black line, respectively: in Figure 5a). On the basis of this discussion, the bands observed after evacuating at RT were assignable to the adsorbed species in moderate strength, irreversibly adsorbed species that were formed through the adsorption that occurred at *ca.* 0.004 Torr. Therefore, the finding of two kinds of bands at 266 and 240 $cm^{-1}$ indicated the presence of at least two types of adsorption sites. On the basis of the reports by Baker *et al.* and Jasra *et al*, we assigned the latter band observed at 240 $cm^{-1}$ to the cation-framework vibrational mode caused by the $Ca^{2+}$ ion exchanged on the 6-MR.[78,79] It should be concluded from the above that in the NaCaA-85 sample, the band at 240 $cm^{-1}$ is shifted toward 203 $cm^{-1}$, which is caused by the interaction of the $Ca^{2+}$ ion exchanged on the 6-MR with $CO_2$. On the other hand, there are so far completely lacking in the assignment of the band observed around 266 $cm^{-1}$ in metal ion-exchanged A-type zeolite as the ion-exchangeable site. These findings are the first indication of the existence of the new type of site in the NaCaA-85 sample prepared in this work. In addition, we must focus on the following points; both bands observed at 266 and 240 $cm^{-1}$ shift toward a lower wave-number side through interaction with $CO_2$: 225 and 203 $cm^{-1}$, respectively, and both bands remain unchanged after the subsequent evacuation of the sample exposed to $CO_2$ vapour at RT for 30 min (Figure 5a, blue line, and Figure SI-4b), and were desorbed concurrently by evacuation at 423 K (Figure 5a, green line). Considering the far-IR data obtained in both the adsorption and desorption processes, the two kinds of sites behave as if they simultaneously interacted with $CO_2$. In addition, on the basis of the adsorption data, it is reasonable to consider that the $CO_2$ molecule is irreversibly adsorbed (60 kJ $mol^{-1}$), and also that the evacuation at 423 K regenerates the original ion-exchanged state (to be shown later). It follows from the changing behaviour of the spectra that these two sites behave in exactly same fashion for the coming $CO_2$ molecule at RT and also in the desorption stage, indicating that the two types of adsorption sites work simultaneously as active sites for $CO_2$ adsorption. To meet these requirements strictly, it is reasonable to assume that the $Ca^{2+}$ ion exchanged on the 8-MR is the most likely site that functions as an effective site together with the closely spaced $Ca^{2+}$ ion exchanged on the 6-MR, leading to the idea that the $CO_2$ molecule is simultaneously pinned by two types of ion-exchanged sites consisting of both the 6- and 8-MRs. This conclusion is also well supported from the results derived from the DFT calculation, which will be shortly described in the next part. The respective spectra for both CaA-78 and NaA samples after $CO_2$ adsorption at RT show little change after the $CO_2$ adsorption at RT in comparison with the case of the NaCaA-85 sample: (Figures 5b, c and SI-4c). As a result, it is entirely fair to say that the cation-vibrational modes found in the far-IR region provide important information to construct the adsorption model, eventually give information for developing adsorbents working in the lower pressure region of $CO_2$. The specific bridging between $Ca^{2+}$ ions situated on both the 6- and 8-MRs is the origin of the development

caused by the present system: the singular $CO_2$ adsorbed species found in the lower pressure region.[85] In view of all discussions given above, we tentatively depicted the reason for the improved $CO_2$-capture performance observed for the NaCaA-85 sample as follows. A large amount of ion-exchanged $Ca^{2+}$ ions afford the sites which are essential for the formation of a $CO_2$ molecule simultaneously pinned by two $Ca^{2+}$ ions positioned on the two types of exchangeable sites composed of 8– and 6–MRs in 5A–type zeolite, resulting in the increase in the adsorption amounts observed in the lower pressure region. These ion-exchangeable sites may be formed with higher priority beyond a certain threshold value of the ion-exchange capacity.

In addition, the band observed between 250 and 150 $cm^{-1}$, which was also observed for the NaA sample, is due to the Na ion exchanged in the 6-MR (230 $cm^{-1}$) and 8-MR (170 $cm^{-1}$), respectively.[78,79] These bands were scarcely observed for the NaCaA-85 sample, suggesting that the $Na^+$ ion scarcely exists in this NaCaA-85 sample or only small amounts of it remain.

For further information, similar models have been reported to date, although these are restricted to experiments performed at lower temperatures on weakly interacted physisorbed systems. The bond lengths of $M_A^{n+}$–O and/or $M_B^{n+}$–O in the $M_A^{n+}$–(O–C–O)–$M_B^{n+}$ species are too long to fall into the category of the systems where the irreversible adsorption is taking place. In some studies, the neutron diffraction (ND) method has been used to clarify the adsorbed states of $CO_2$. Judging from the sensitivity of this method, the dominant target is generally limited to the analysis of the physisorbed species.[69,86] Therefore, the ND method is not suitable for determining the state of $CO_2$ adsorbed in the lower pressure region of not more than 5000 ppm, i.e., a singular phenomenon found in the present work. By contrast, the far-IR method combined with the DFT calculation method has enabled us to obtain important information on the adsorbed states arising from its high detection sensitivity even if the case of it in limited amount, in comparison with another ND method.

**(b) DFT discussion on the spectra observed in the far-IR region**

Recent progress in calculation was achieved with the DFT calculation method and provided reliable information on the vibrational modes; we were able to create images of respective characteristic modes as movies. For this purpose, a model had to be constructed to implement the DFT calculation on our system on the basis of our experimental data. At this stage, the model should be capable of explaining the following experimental data. The most striking aspect of the present result was, first, that the zeolite material without a specific basic property exhibited an effective adsorption feature at RT even in the lower pressure region. Second, the adsorption specificity was only seen in a CaA-type zeolite with the higher exchanging level: NaCaA-85. Third, the adsorption heats were not as large as found in cases with strong chemisorption, i.e., this species was relatively easily desorbed below 423 K. These findings indicated that the driving force working in this system was quite different from that caused by the general acid–base

interaction.[87] Furthermore, we must explain the singular discrimination between $CO_2$ and $N_2$, as well as $CH_4$, which have almost similar kinetic diameters. This information will be provided later in this article. To meet these requirements strictly, we constructed a model made up of a $CO_2$ molecule pinned between two $Ca^{2+}$ ions positioned on two types of exchangeable sites composed of 8- and 6-MRs, as found in the far-IR measurement. The model adopted in the present system is shown in Scheme 1. On the basis of the constructed model, the IR bands were calculated before and after $CO_2$ adsorption with the DFT calculation method. We focused on the band observed around 250 $cm^{-1}$, aiming to justify the proposed model through the reproduction of these far-IR data by the DFT method. The derived results based on this calculation are presented in Figures 6a and b. For easy and detailed comparisons, the difference spectra are also presented in Figure SI-4d. Overall, the data obtained by DFT calculation matched our findings derived from the far-IR experiment (Figure 6b and the difference spectra in Figures SI-4b which is experimental data and 4d which is obtained with the aid of DFT calculation). This assignment was also supported by combining with the data for the mid-IR region as discussed in the next section.

**(c) Study based on the mid-IR spectra**

We intend to obtain additional information on the suitability of the proposed model from the viewpoint of the results derived from the measurements in the mid-IR region. However, two specific difficulties were encountered in determining the adsorbed states of $CO_2$ on the NaCaA-85 sample. The first one stemmed from the fact that the amount of $CO_2$ adsorbed was too large to hold the absorption within the suitable range in the case of the *in situ* experiment using the self-supporting disk. The second was the difficulty in controlling an accurate pressure under 0.01 Torr levels, because of the unprecedented behaviour occurring around the extremely low pressure region of 400 ppm observed in the present case. These difficulties were overcome in two ways. The first was using a mixture of isotope gases composed of both $^{12}CO_2$ and $^{13}CO_2$ with roughly a 1:1 composition. Based on the data described above, the second way was to mainly focus on the desorption process of the residual species on the surface with exposure to a few Torr of $CO_2$ gas and subsequently evacuating from 300 K to 423 K to focus on the bonding states of the irreversibly adsorbed $CO_2$ species. Under such circumstances, we examined the sample that gave the most specific $CO_2$ adsorption property, i.e., the NaCaA-85 sample. On this sample, we focused on the asymmetric vibration of the adsorbed $CO_2$. In line with this strategy, the sample was first evacuated at 723 K. No absorption band was observed in the asymmetric region after evacuation at 723 K (Figures 7a and b). On this sample, the isotropically mixed $CO_2$ gas ($^{12}CO_2$ + $^{13}CO_2$ at the ratio of *ca*. 1 to 1) at *ca.* 2 Torr was adsorbed at RT. After this treatment, the sample was re-evacuated at RT, which gave very strong bands around 2360 and 2285 $cm^{-1}$ for adsorbed $^{12}CO_2$ and $^{13}CO_2$, respectively, although these bands were observed as saturated bands in both regions, (Figures 7a and b: depicted by the solid blue line). A careful examination of these spectra revealed

a noticeable shoulder band at 2299 $cm^{-1}$ for the adsorbed $^{13}CO_2$ species. The latter band loses its intensity through subsequent evacuation at 323 K, giving the characteristic sharp band at 2289 $cm^{-1}$ and at 2356 $cm^{-1}$; these were assigned to the irreversibly adsorbed $^{13}CO_2$ and $^{12}CO_2$ species, respectively. By increasing the evacuation temperatures, the intensities of these bands decreased, and finally were lost after evacuation at 423 K. These observations matched the TPD results well (Figure 4), and also the isotherm data in Figure 1 and the far-IR data (Figure 5), indicating that the strongly irreversibly-adsorbed species provided the asymmetric vibration band at 2289 $cm^{-1}$ for $^{13}CO_2$, and at 2356 $cm^{-1}$ for $^{12}CO_2$. On the isotopic basis of these results, the peak at 2299 $cm^{-1}$ due to weakly irreversibly-adsorbed $^{13}CO_2$ converts to 2366 $cm^{-1}$ on the $^{12}CO_2$ basis by multiplying with the factor of 1.029 (= 2356/2289). To verify the IR data in the initial adsorption process in the extremely low pressure region, the $^{12}CO_2$ adsorption process was also investigated, resulting in the observation of the band at 2367 $cm^{-1}$ under an equilibrium pressure of *ca.* 0.003 Torr (Figures 7c and SI-5). The band had a skirt toward the lower wave-number region (Figure 7c). A deconvolution analysis was performed on this spectrum by assuming two kinds of band, including the one at 2367 $cm^{-1}$. The resultant spectra consisted of two components at 2367 $cm^{-1}$ and 2357 $cm^{-1}$ (Figure SI-5). Thus, the obtained experimental results were confirmed by comparison with the calculated data. For assignment, the calculation was performed on three kinds of adsorption models: a $CO_2$ molecule adsorbed on either 8- or 6-MRs, and also a $CO_2$ molecule bridging between two $Ca^{2+}$ ions positioned on two types of exchangeable sites composed of 8- and 6-MRs. The calculated bands for the respective models were evaluated by the DFT calculation method (Figure 7d). These findings were also supported on the basis of DFT calculation using the proposed model: the adsorbed $CO_2$ by simultaneously pinned by the $Ca^{2+}$ ions positioned on the 8-MR and 6-MR which gives the value of 2357 $cm^{-1}$. The resultant calculation supported our proposed model well. By contrast, the $CO_2$ adsorbed singly on 8- or 6-MR was evaluated to be the interacting $CO_2$ species, 2368 or 2361 $cm^{-1}$, respectively. These mid-IR data further justified our proposed model.

The model used in this work was similar to that reported by Nachtigall and Areán's group, which was used for explaining the CO adsorption phenomenon observed in the CaA-type zeolite system.[88] They concluded that the bridged CO species formed between a $Ca^{2+}$ ion located on an 8-MR and another one on a nearby 6-MR. It is characterized by $\nu_{CO}$ in the range 2183–2188 $cm^{-1}$, and the band at 2183 $cm^{-1}$ was derived from these authors' computational study using the periodic DFT level calculation. In our case, the measurements for the CO adsorption at RT were examined on the NaCaA-85 sample and the band centred at 2183 $cm^{-1}$ was observed (Figure SI-6). Therefore, it seems appropriate to say that these results also strongly point to the validity of our proposed model for the specific $CO_2$ adsorption observed in the present work. Čejka's group also addressed the adsorption of $CO_2$ in the NaA sample.[89] They also explained the $CO_2$

adsorption behaviour on the NaA sample by using a similar model, although there is no description about the specific adsorption property in the low pressure region that is addressed in the present work.

**(III) Specificity of the NaCaA-85 sample for $CO_2$ adsorption: peculiar and selective adsorption**

**(a) Regeneration of the Sample through heat treatment at 423 K**

To verify the regeneration process of the NaCaA-85 sample, the adsorption isotherms were measured. First, the sample was evacuated at 723 K, followed by an adsorption measurement at 298 K at an equilibrium pressure of *ca.* 80 Torr; this was the first adsorption. Next, the second adsorption isotherm was examined for the sample re-evacuated at 298 K. Thus treated sample was again re-evacuated at 423 K. The measurement of the adsorption isotherm was performed at 298 K successively. The results of these processes are shown in **Figure SI-7**. In comparison to the adsorption amounts observed in the original ($1^{st}$) adsorption measurement process, the $2^{nd}$ regeneration process is slightly decreases in amounts. After the third time, the adsorbed amounts were not essentially altered. Focused on the lower equilibrium pressure region, the $2^{nd}$ indicates slight decrease, but the amounts do not exhibit further decrease after the $2^{nd}$ process. In addition, the adsorbed amounts exhibit sharp increase in all samples in the lower pressure region and their values are obviously larger in comparison with the data for the CaA-78 sample observed in the first adsorption process which is same as the data given by green line in Figure 1a. On the basis of these observations, it seems reasonable to suppose that this material finds advantage for the $CO_2$ adsorbent functioning under lower pressure region. Therefore, it is not too far the truth to say that the sample almost regenerated to its original state through the evacuation at 423 K.

**(b) The adsorption behaviour of $CO_2$ in comparison with that observed for other gases**

Zeolites have not yet been recognized as the good materials for $CO_2$ capture directly from air at RT, because of their small adsorption capacity in the low pressure region and poor selectivity over $N_2$.[55,56] Thus far, zeolites have been used as the efficient material functioning in the higher pressure of $CO_2$ but not been of interest in the lower pressure region.[55,56] To date, there have been no studies on zeolite samples, which work as the excellent adsorbent even under lower pressures. Sayari *et al*. have also indicated the need for the development of zeolites with higher selectivity for $CO_2/N_2$.[8] Considering the specificity found in our system in the low pressure region, the adsorption isotherms for various gases such as $N_2$, $H_2$, $O_2$, and $CH_4$ at 298 K were measured on the NaCaA-85 sample to confirm the specificity for $CO_2$ (Figure 8). Judging from this figure, this sample exhibited superior selectivity for $CO_2$, compared with other gases in both the lower and medium pressure regions.

**(c) Separation of $CO_2$ in the actual pressure system**

On the basis of the selectivity for $CO_2$ of the NaCaA-85 sample (Figure 8), the adsorption impurity separating behaviour of this sample was assessed under the condition given in the experimental section using the model gas composed of 0.04% $CO_2$, 20% $O_2$ and 79.96% $N_2$, which mimicked ambient air, although $H_2O$ was not included in the mixture gas. In this experiment, the sample evacuated at 723 K was exposed to the model gas at 300 K for 120 min. The changes in $CO_2$ amount measured in the adsorption and the succeeding desorption process by increasing the temperature through purging He were examined with the aid of the mass spectrum. In this case, the desorbed gases were detected by the mass spectroscopic method: the mass numbers of 28 and 14 for $N_2$, 32 for $O_2$ and 44 for $CO_2$, respectively. The desorbed gas detected was only $CO_2$ in these experiments; the adsorption and desorption processes examined by *m*/*z* of 44 are depicted in Figure 9. The first process in this figure was assigned to the adsorption process of $CO_2$ around 300 K, followed by desorption of the weakly irreversibly-adsorbed $CO_2$ species to *ca.* 343 K (70 ℃). The final distinctly desorbed species was observed at around 375 K (102 ℃) which is due to the strongly irreversibly-adsorbed $CO_2$ species. The amounts desorbed irreversibly are evaluated to be 0.487 mmol $g^{-1}$ (= *ca.* 10.9 $cm^3$ $g^{-1}$) from the areas of two kinds of bands observed in the breakthrough curve. It is entirely fair to say that this value is well corresponding to the value evaluated from the difference between the adsorbed amounts obtained from the 1st and 2nd adsorption isotherms. In addition, it is generally recognized that the separation of $CO_2$ from $CH_4$ is difficult in gases, because both gases have similar molecular nature in polarizability and molecular size: Table SI-1a. Therefore, we try to separate $CO_2$ in the system including $CH_4$, by considering the results of the isotherm data depicted in Figure 8. The adsorption impurity separating behaviour was assessed under the same condition shown above by using the model gas composed of 0.04% $CO_2$, 0.04% $CH_4$, 20% $O_2$ and 79.92% $N_2$ (without $H_2O$). The change in $CO_2$ amount measured in the adsorption and the succeeding desorption process by increasing the temperature through purging with $N_2$ was examined. In this case, the desorbed gases were detected by the mass spectroscopic method: the mass numbers 16 and 15 for $CH_4$, 32 for $O_2$ and 44 for $CO_2$, respectively. The desorbed gas detected was only $CO_2$ in these experiments; the outcome is also depicted in Figure SI-8. The first process was assigned to the adsorption process of $CO_2$ around 300 K, followed by desorption of the weakly irreversibly-adsorbed $CO_2$ species to *ca.* 343 K (70 ℃). The final distinctly desorbed species was observed at around 381 K (108 ℃) which is due to the strongly irreversibly-adsorbed $CO_2$ species; a high separation performance for $CO_2$ is clearly ascertained. The amounts desorbed irreversibly are evaluated to be 0.484 mmol $g^{-1}$ (= *ca.* 10.8 $cm^3$ $g^{-1}$) from the areas of two kinds of bands observed in the breakthrough curve. These experimental results prove clearly that the selective adsorption of $CO_2$ occurred in the present system at 300 K even in a gas mixture mimicking atmospheric gas. From these remarks, one

general point becomes very clear: the NaCaA-85 sample is a prominent candidate material for the selective $CO_2$ adsorbent functioning in DAC conditions.

**Conclusions**

The development of adsorbents having efficient adsorptive and selective properties for $CO_2$ that function at RT and in the lower pressures is indispensable for aiming at DAC of $CO_2$. In this work, we have succeeded in conferring an outstanding adsorption feature for $CO_2$ onto the $Ca^{2+}$ ion-exchanged NaA-type zeolite sample, i.e., NaCaA-85 (where the last number indicates the ion-exchange capacity by $Ca^{2+}$), which gives the following adsorption properties: the adsorbed amount of 0.75 mmol $g^{-1}$ at 0.01 Torr (with a "characteristic gentle step" in the adsorption isotherm around 0.004 Torr) and an adsorption energy of 60 kJ $mol^{-1}$, 1.8 mmol $g^{-1}$ and *ca.* 52 kJ $mol^{-1}$ at 0.3 Torr (400 ppm), and 3.2 mmol $g^{-1}$ at 3.8 Torr (5000 ppm), which is the best adsorption result reported to date, and adsorption energy of 48 kJ $mol^{-1}$, respectively. To obtain the information on the role of exchanged $Ca^{2+}$ ions for the specific $CO_2$ adsorption observed in the NaCaA-85 zeolite at RT, far-IR spectra were measured in this system by taking advantage of SOR light, which is bright, stable, and reproducible, compared with the conventional infrared sources, leading to the definite detection of the changes in the cation-vibrational modes due to the $Ca^{2+}$-zeolite vibration through the adsorption of $CO_2$ at RT. As a result, the $Ca^{2+}$-framework vibration modes for the NaCaA-85 sample were observed at 266 and 246 $cm^{-1}$, and shifted toward the lower wave-number sides, i.e., 225 and 203 $cm^{-1}$, after $CO_2$ adsorption at RT, respectively, whereas these distinct changes in far-IR spectra before and after $CO_2$ adsorption were not recognized in both purchased CaA-78 and NaA samples. The $Ca^{2+}$ ions that were active in the $CO_2$ adsorption were assigned to the exchangeable ions positioned on the 8- and 6-MRs, respectively. The observed characteristic property was reasonably explained by the model made up by a $CO_2$ molecule bridging between two $Ca^{2+}$ ions positioned on two types of exchangeable sites composed of 8- and 6-MRs, which is well supported by the DFT calculation method. The simultaneous existence of the two types of exchangeable sites found in this work is indispensable for the singular $CO_2$ adsorption behaviour observed in the low pressure region. It was also found that the adsorption property for $CO_2$ at RT was superior compared with the adsorption of $CH_4$, $N_2$ and $O_2$. The separation properties were examined by measuring the breakthrough curve using a gas mixture mimicking the atmosphere, which verified the superior separation feature from $N_2$, $O_2$ and $CH_4$. The NaCaA-85 sample presented the selective feature for trace $CO_2$ capture and easy regeneration; this characteristically adsorbed $CO_2$ species was completely desorbed through evacuation at 423 K. In addition, the NaCaA-85 sample was easily regenerated by re-evacuation at 423 K and the specific adsorption properties were almost recovered even after $5^{th}$-times regeneration treatments of the sample after each $CO_2$-adsorption treatment. These unique

properties of this sample have the potential for developing efficient adsorbent functioning under lower pressure $CO_2$ in a semi-closed space, i.e., for the purification of air, and also for $CO_2$ capture in DAC conditions, although dehydration process before $CO_2$ separation may be required when atmospheric air is humid.

## ■ Associated content

Electronic supplementary information (ESI) available. See DOI: 10.1039/…….

Experimental details, physical parameters, comparison of the adsorbed amounts of $CO_2$ on various samples, CO adsorption isotherm, far-IR spectra, difference spectra in far-IR region (experimental and theoretical data), IR spectra in mid-IR region, IR spectra of CO, isotherms after the regeneration processes, breakthrough curve of $CO_2$ measured by use of a gas mixture composed of $CO_2$, $CH_4$, $O_2$ and $N_2$, and DTG data of NaCaA-85 sample.

## ■ Author information

Corresponding Author

***Professor Dr. Yasushige Kuroda**—Department of Chemistry, Graduate School of Natural Science and Technology, Okayama University, 3-1-1 Tsushima-naka, Kita-ku, Okayama 700-8530, Japan; E-mail: kuroda@cc.okayama-u.ac.jp

Present address

[+]**Dr. Akira Oda** —Material Chemistry, Graduate School of Engineering, Nagoya University, Furo-cho, Chikusa-ku, Nagoya, 464-8603, Japan; E-mail: akira@chembio.nagoya-u.ac.jp

## ■ Conflicts of interest

There are no conflicts to declare.

## ■ Acknowledgements

We would like to thank Ms. Yap Mee Lin for her contribution to the development of the sample preparation method and thanks are due to Mr. Yuta Sakamoto for his assistance and support in experimental data acquisition in the measurements of isotherms and heats of adsorption. The far-IR measurements were carried out at the BL43IR of SPring-8 with the approval of the Japan Synchrotron Radiation Research Institute (JASRI): Proposal Nos. 2017B1363, 2018A1299 and 2018B1386. We wish to express our gratitude to JASCO Corporation (JAPAN) for giving us a chance to carry out preliminary far-IR experiment for examining the possibility of the far-IR measurement in our systems. The authors also thank to Mr. Sato and Mr. Fujiwara in the glassblowing workshop of Hiroshima University for technical assistance in making *in situ* cell for far-IR measurements. Thanks are also due to Microtrac-BEL Corporation (JAPAN) for supporting us in the experiment of the Breakthrough-curve measurements. One of the authors (Y. K.) gratefully acknowledges the financial supports from Japan Society of Promotion Science (Grant-in-Aid for Scientific Research B: No. 16H04118 and Scientific Research C: No.

19K05499). Dr. A. O. specially acknowledges supports from the Japan Society for the Promotion of Science (Research Fellowship for Young Scientists, DC1 and PD) and also from the Japan Science and Technology Agency.

## References and Notes


1 WMO Greenhouse Gas Bulletin, 2019, **No. 15**, 1–8.

2 R. Monastersky, *Nature*, 2013, **497**, 13–14.

3 W. D. Jones, *J. Am. Chem. Soc.,* 2020, **142**, 4955–4957.

4 G. A. Olah, A. Goeppert, G. K. Surya Prakash, Beyond Oil and Gas: The Methanol Economy. 2nd updated and enlarged Ed. Wiley-VCH Verlag GmbH & Co. KGaA, Weinheim, 2009

5 D. S. Sholl and R. P. Lively, *Nature*, 2016, **532**, 435–437.

6 D. W. Keith, *Science*, 2009, **325**, 1654–1655.

7 C. Hepburn, E. Adlen, J. Beddington, E. A. Carter, S. Fuss, N. Mac Dowell, J. C. Minx, P. Smith, C. K. Williams, *Nature*, 2019, **575**, 87–97.

8 A. Sayari, Y. Belmabkhout and R. Serna-Guerrero, *Chem Eng. J.*, 2011, **171**, 760–774.

9 J. Kim, L.-C. Lin, J. A. Swisher, M. Haranczyk and B. Smit, *J. Am. Chem. Soc.*, 2012, **134**, 18940–18943.

10 O. Cheung and N. Niklas Hedin, *RSC Adv.*, 2014, **4**, 14480–14494.

11 D. G. Madden, H. S. Scott, A. Kumar, K.-J. Chen, R. Sanii, A. Bajpai, M. Lisi, T. Curtin, J. J. Perry, and M. J. Zaworotko, *Philos. Trans. A Math. Phys. Eng. Sci.,* 2017, **375**, 20160025.

12 Z. Shi, Y. Tao, J. Wu, C. Zhang, H. He, L. Long, Y. Lee, T. Li and Y.-B. Zhang, *J. Am. Chem. Soc.* 2020, **142**, 2750−2754.

13 G. T. Rochelle, *Science*, 2009, **325**, 1652–1654.

14 J. Wang, L. Huang, R. Yang, Z. Zhang, J. Wu, Y. Gao, Q. Wang, D. O'Hare and Z. Zhong, *Energy Environ. Sci*., 2014, **7**, 3478–3518.

15 S. Choi, J. H. Drese and C. W. Jones, *ChemSusChem*, 2009, **2**, 796–854.

16 D. M. D'Alessandro, B. Smit and J. R. Long, *Angew. Chem. Int. Ed.*, 2010, **49**, 6058–6082.

17 J. G. Vitillo, *RSC Adv.*, 2015, **5**, 36192–36239.

18 S. Cavenati, C. A. Grande and A. E. Rodrigues, *J. Chem. Eng. Data*, 2004, **49**, 1095–1101.

19 D. Bonenfant, M. Kharoune, P. Niquette, M. Mimeault and R. Hausler, *Sci. Technol. Adv. Mater.*, 2008, **9**, 013007(7).

20 L. Hauchhum and P. Mahanta, *Int. J. Energy Environ. Eng.*, 2014, **5**, 349–356.

21 Q. Wang, J. Luo, Z. Zhong and A. Borgna, *Energy Environ. Sci.*, 2011, 4, 42–55.

22 M. D. Jennifer Law, In-Flight Carbon Dioxide Exposures and Related Symptoms: Association, Susceptibility, and Operational Implications, NASA/TP–2010– 216126

23 T. A. Jacobson, J. S. Kler, M. T. Hernke, R. K. Braun, K. C. Meyer and W. E. Funk, *Nat. Sustain.*, 2019, **2**, 691–701.

24 The chemicals or substances contained in the revision include all substances for which the National Institute for Occupational Safety and Health (NIOSH) has recommended exposure limits (RELs);

https://www.cdc.gov/niosh/idlh/124389.html.

25 A. Kumar, D. G. Madden, M. Lusi, K.-J. Chen, E. A. Daniels, T. Curtin, J. J. Perry IV and M. J. Zaworotko, *Angew. Chem. Int. Ed.*, 2015, **54**, 14372–14377.

26 D. W. Keith, G. Holmes, D. St. Angelo and K. Heidel, *Joule*, 2018, **2**, 1573–1594.

27 C. Beuttler, L. Louise Charles and J. Wurzbacher, *Front. Clim.*, 2019, **1**, article 10.

28 E. S. Sanz-Pérez, C. R. Murdock, S. A. Didas and C. W. Jones, *Chem. Rev.*, 2016, **116**, 11840–781.

29 F. Inagaki, C. Matsumoto, T. Iwata and C. Mukai, *J. Am. Chem. Soc.*, 2017, **139**, 4639–4642.

30 X. Shi, H. Xiao, H. Azarabadi, J. Song, X. Wu, X. Chen and K. S. Lackner, *Angew. Chem. Int. Ed.* 2020, 59, 6984–7006.

31 N. J. Williams, C. A. Seipp, F. M. Brethomé, Y.–Z. Ma, A. S. Ivanov, V. S. Bryantsev, M. K. Kidder, H. J. Martin, E. Holguin, K. A. Garrabrant and R. Custelcean, *Chem*, 2019, **5**, 719–730.

32 S. K. Shukla, S. G. Khokarale, T. Q. Bui and J.-P. T. Mikkola, f*rontiers in Materials*, 2019, **6**, Article 42.

33 S. Zeng, X. Zhang, L. Bai, X. Zhang, H. Wang, J. Wang, D. Bao, M. Li, X. Liu and S. Zhang, *Chem. Rev.,* 2017, **117**, 9625−9673.

34 T. M. McDonald, W. R. Lee, J. A. Mason, B. M. Wiers, C. S. Hong and J. R. Long, *J. Am. Chem. Soc.* 2012, **134**, 7056−7065.

35 J. P. Sculley and H.-C. Zhou, *Angew. Chem. Int. Ed.,* 2012, **51**, 12660–12661.

36 Y. Kuwahara, D.-Y. Kang, J. R. Copeland, N. A. Brunelli, S. A, Didas, P. Bollini, C. Sievers, T. Kamegawa, H. Yamashita and C. W. Jones, *J. Am. Chem. Soc.*, 2012, **134**, 10757–10760.

37 M. Kang, D. W. Kang and C. S. Hong, *Dalton Trans.*, 2019, **48**, 2263–2270.

38 W. R. Lee, S. Y. Hwang, D. W. Ryu, K. S, Lim, S. S. Han, D. Moon, J. Choi and C. S. Hong, *Energy Environ. Sci*., 2014, **7**, 744–751.

39 W. R. Lee, H. Hyuna Jo, L.-M. Yang, H. Lee., D. W. Ryu, K. S. Lim, J. H. Song, D. Y. Min, S. S. Han, J. G. Seo, Y. K. Park, D. Moon and C. S. Hong, *Chem. Sci.,* 2015, **6**, 3697–3705.

40 L. A. Darunte, T. Sen, C. Bhawanani, K. S. Walton, D. S. Sholl, M. J. Realff and C. W. Jones, *Ind. Eng. Chem. Res.,* 2019, **58**, 366–377.

41 J.–R. Li, R. J. Kuppler and H.–C. Zhou, *Chem. Soc. Rev.,* 2009, **38**, 1477–1504.

42 K. Sumida, D. L. Rogow, J. A. Mason, T. M. McDonald, E. D. Bloch, Z. R. Herm, T.-H. Bae and J. R. Long, *Chem. Rev.*, 2012, **112**, 724–781.

43 O. Shekhah, Y. Belmabkhout, Z. Chen, V. Guillerm, A. Cairns, K. Adil and M. Eddaoudi, *Nature Commun.,* 2014, **5**, 4228.

44 P. M. Bhatt, Y. Belmabkhout, A. Cadiau, K. Adil, O. Shekhah, A. Shkurenko, L. J. Barbour and M. A. Eddaoudi, *J. Am. Chem. Soc.,* 2016, **138**, 9301−9307.

45 H. Jo, W. R. Lee, N. W. Kim, H. Jung, K. S. Lim, J. E. Kim, D. W. Kang, H. Lee, V. Hiremath, J. G. Seo, H. Jin, D. Moon, S. S. Han and C. S. Hong, *ChemSusChem*, 2017, **10**, 541–550.

46 A. Kumar, C. Hua, D. G. Madden, D. O'Nolan, K.–J. Chen, L.–A. J. Keane, J. J. Perry IV and M. J. Zaworotko, *Chem. Commun.*, 2017, **53**, 5946–5949.

47 C. A. Trickett, A. Helal, B. A. Al-Maythalony, Z. H. Yamani, K. E. Cordova and O. M. Yaghi, *Nat. Rev. Mater.,* 2017, **2**, 17045.

48 A. Karmakar, P. Samanta, A. V. Desai and S. K. Ghosh, *Acc. Chem. Res.,* 2017, **50**, 2457−2469.

49 X. Song, M. Zhang, C. Chen, J. Duan, W. Zhang, Y. Pan and J. Bai, *J. Am. Chem. Soc.,* 2019, **141**, 14539−14543.

50 A. Looney, R. Han, K. McNeill and G. Parkin, *J. Am. Chem. Soc.,* 1993, **115**, 4690–4697.

51 W. Sattler and G. Parkin, *Chem. Sci.,* 2012, **3**, 2015–2019.

52 A. M. Wright, Z. Wu, G. Zhang, J. L. Mancuso, R. J. Comito, R. W. Day, C. H. Hendon, J. T. Miller and M. Dinc, *Chem*, 2018, **4**, 2894–2901.

53 C. Jin, S. Zhang, Z. Zhang and Y. Chen, *Inorg Chem.,* 2018, **57**, 2169−2174

54 C. E. Bien, K. K. Chen, S.-C. Chien, B. R. Reiner, L.-C. Lin, C. R. Wade and W. S. Winston Ho, *J. Am. Chem. Soc.,* 2018, **140**, 12662−12666.

55 F. Akhtar, Q. Liu, N. Hedin and L. Bergström, *Energy Environ. Sci.*, 2012, **5**, 7664–7673.

56 M. R. Hudson, W. L. Queen, J. A. Mason, D. W. Fickel, R. L. Lobo and C. M. Brown, *J. Am. Chem. Soc.,* 2012, **134**, 1970–1973.

57 P. Nugent, Y. Belmabkhout, S. D. Burd, A. J. Cairns, R. Luebke, K. Forrest, T. Pham, S. Ma, B. Space, L. Wojtas, M. Eddaoudi and M. J. Zaworotko, *Nature,* **2013**, *495*, 80–84.

58 M. Oschatz and M. Antonietti, *Energy Environ. Sci.*, 2018, **11**, 57–706.

59 A. Itadani, A. Oda, H. Torigoe, T. Ohkubo, M. Sato, H. Kobayashi and Y. Kuroda, *ACS Appl. Mater. Interfaces*, 2016, **8**, 8821–8833.

60 S. J. Datta, C. Khumnoon, Z. H. Lee, W. K. Moon, S. Docao, T. H. Nguyen, I. C. Hwang, D. Moon, P. Oleybujiv, O. Terasaki and K. B. Yoon, *Science*, 2015, **350(6258**), 302–306.

61 P. M. Bhatt, Y. Belmabkhout, A. Cadiau, K. Adil, O. Shekhah, A. Shkurenko, L. J. Barbour and M. A. Eddaoudi, *J. Am. Chem. Soc.,* 2016, **138**, 9301−9307.

62 S. Mukherjee, N. Sikdar, D. O'Nolan, D. M. Franz, V. Gascón, A. Kumar, N. Kumar, H. S. Scott, D. G. Madden, P. E. Kruger, B. Space and M. J. Zaworotko, *Sci. Adv.*, 2019, **5**, eaax9171 (1–7).

63 K.-M. Lee, Y.-H. Lim, C.-J. Park and Y.-M. Jo, *Ind. Eng. Chem. Res.*, 2012, **51**, 1355–1363.

64 A. G. Arévalo-Hidalgo, N. E. Almodóvar-Arbelo and A. J. Hernández-Maldonado, *Ind. Eng. Chem. Res.*, 2011, **50**, 10259–10269.

65 R. D. Shannon, *Acta Cryst.,* 1976, **A32**, 751−767.

66 L. M. Mulloth and J. E. Finn, report NASA/TM-1998-208752: Moffett Fields, CA, 1998.

67 Y. Wang and D. LeVan, *J. Chem Eng. Data*, 2009, **54**, 2839–2844.

68 Q. H. Dirar and K. F. Loughlin, *Adsorption*, 2013, **19**, 1149–1163.

69 T.-H. Bae, M. R. Hudson, J. A. Mason, W. L. Queen, J. J. Dutton, K. Sumida, K. J. Micklashi, S. S.

Kaye, C. M. Brown and J. R. Long, *Energy Environ. Sci*., 2013, **6**, 128–138.

70 F. W. Miranda da Silva, Maia, A. S. D´ebora, R. S. Oliveira, J. C. Moreno-Piraj´an, K. Sapag, C. L. Cavalcante, G. Zgrablich and D. C. S. Azevedo, *Can. J. Chem. Eng.*, 2012, **92**, 1372–1380.

71 R. Arrigo, M. Hävecker, S. Wrabetz, R. Blume, M. Lerch, J. McGregor, E. P. J. Parrott, J. A. Zeitler, L. F. Gladden, A. Knop-Gericke, R. Schlögl and D. S. Su, *J. Am. Chem. Soc.,* 2010, **132**, 9616–9630.

72 W. Mozgawa, M. Handke and W. Jastzębski, *J. Mol. Struct.,* 2004, **704**, 247–257.

73 W. Mozgawa, M. Król and K. Barczyk, *CHEMIK*, 2011, **65**, 671–674.

74 M. Król, W. Mozgawa, W. Jastzębski and K. Barczyk, *Micropor. Mesopor. Mater.*, 2012, **156**, 181–188.

75 M. Król, W. Mozgawa and W. Jastzębski, *J. Porous Mater.*, 2016, **23**, 1–9.

76 A. M. Mofrad, C. Peixoto, J. Blumeyer, J. Liu and H. Hunt, H. *J. Phys. Chem. C*, 2018, **122**, 24765–24779.

77 M. D. Baker, J. Godber and G. A. Ozin, *J. Am. Chem. Soc.,* 1985, **107**, 3033–3043.

78 M. D. Baker, J. Godber, K. Helwig and G. A. Ozin, *J. Phys. Chem.*, 1988, **92**, 6017–6024.

79 R. V. Jasra, N. V. Choudary, K. V. Rao, G. C. Pandey and S. G. Bhat, *Chem. Phys. Lett.*, 1993, **211**, 214–219.

80 M. Zahmakıran, Y. Tonbul and S. Özkar, *J. Am. Chem. Soc.,* 2010, **132**, 6541–6549.

81 J. Baumann, R. Beer, G. Calzaferri and B. Waldeck, *J. Phys. Chem.*, 1989, **93**, 2292–2302.

82 E. Garrone, B. Bonelli, C. Lamberti, B. Civalleri, M. Rocchia, P. Roy and C. O. Areán, *J. Chem. Phys.,* 2002, **117**, 10274–10282.

83 Y. Ikemoto, T. Moriwaki, T. Nakano and Y. Nozue, *Infrared Phys. Techn.*, 2006, **49**, 78–81.

84 S. Dalla Bernardina, F. Alabarse, A. Kalinko, P. Roy, M. Chapuisa, N. Vitaa, R. Hienerwadelb, C. Berthomieuc, P. Judeinsteind, J.-M. Zanottid, J. L. Bantigniese, J. Hainesf, J. Catafestaf, G. Creff, L. Manceron and J.-B. Brubach, *Vib. Spectrosc,.* 2014, **75**, 154–161.

85 The accurate position of the exchanged $Ca^{2+}$ ion hasn't clarified yet. We carried out private discussion with Drs. K. Yoshida and Y. Sasaki; they could not specified the positions of the exchanged $Ca^{2+}$ ions within A-type zeolite through the combined methods ab initio DFT calculation and HRTEM together with STEM techniques, as is different from the cases of NaA- and CsA-type zeolites. For NaA and CsA-type zeolites, refer to the following their work: K. Yoshida, K. Toyoura, K. Matsunaga, A. Nakahira, H. Kurata, Y. H. Ikuhara and Y. Sasaki, Y. Atomic sites and stability of $Cs^+$ captured within zeolitic nanocavities. *Sci. Reports*, 2013, **3**, 2457 (DOI: 10.1038/srep02457).

86 S. H. Ogilvie, S. G. Duyker, P. D. Southon, V. K. Peterson and C. J. Kepert, *Chem. Commun.*, 2013, **49**, 9404–9406.

87 In this work, we defined that the adsorbed amounts evaluated from the difference in the 1st and 2nd adsorption amounts, which are the residual $CO_2$ even after evacuating at 298 K of the sample measured the 1st adsorption isotherm. This amount corresponds to the "irreversibly adsorbed $CO_2$ species".

Generally, it can be described that these species may be of a wide range from weak chemisorption to strong chemisorption. The species found in this work show the adsorption energies from 65 kJ/mol to 55 kJ/mol. These values are only slightly larger than those observed for "physisorbed species".[15–17,37,69] Actually, these species found in this work are desorbed after evacuation at 423 K. Therefore, in the present work, we defined these species as "weakly irreversibly-adsorbed species" as well as "strongly irreversibly-adsorbed species. As for the chemisorbed systems, we cited the typical review paper which explained the adsorption-heat data including zeolite systems: N. C.-Martines and J. A. Dumesic, Applications of Adsorption Microcalorimetry to the Study of Heterogeneous Catalysis, *Adv. Catal.*, 1992, **38**, 149–244.

88 A. Pulida, P. Nachtigall, M. R. Delgado and C. O. Areán, *ChemPhysChem*, 2009, **10**, 1058–1065.

89 A. Zukal, C. O. Areán, M. R. Delgado, P. Nachtigall, A. Pulido, J. Mayeravá and J. Čejka, *Micropor. Mesopor. Mater.*, 2011, **146**, 97–105.

Scheme 1.

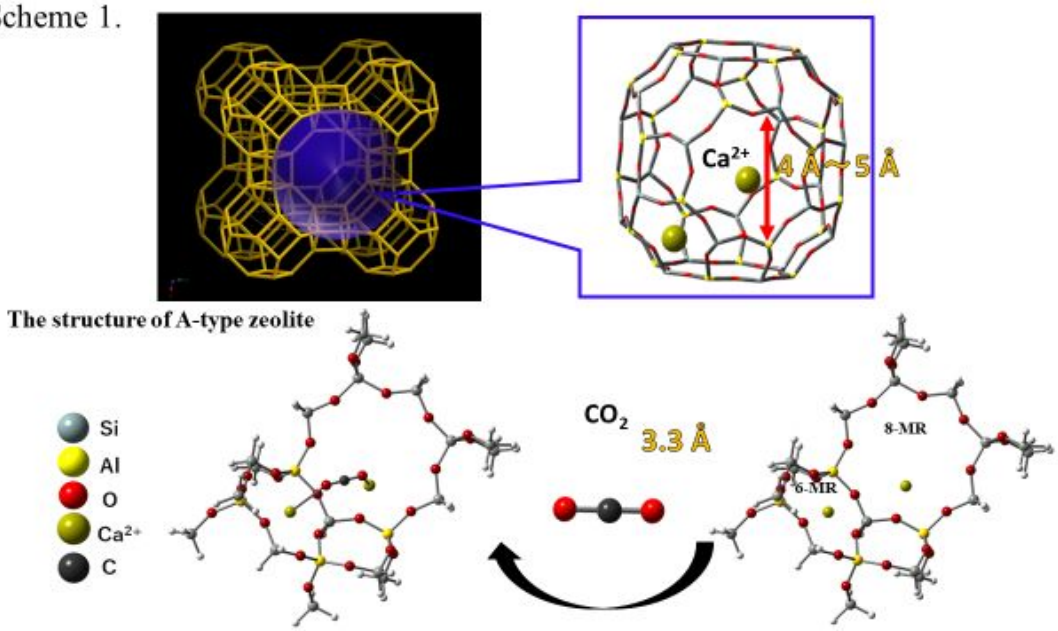
Ca2+
4 Å~5 Å
The structure of A-type zeolite
Si
Al
O
Ca2+
C
CO2
3.3 Å
8-MR
6-MR

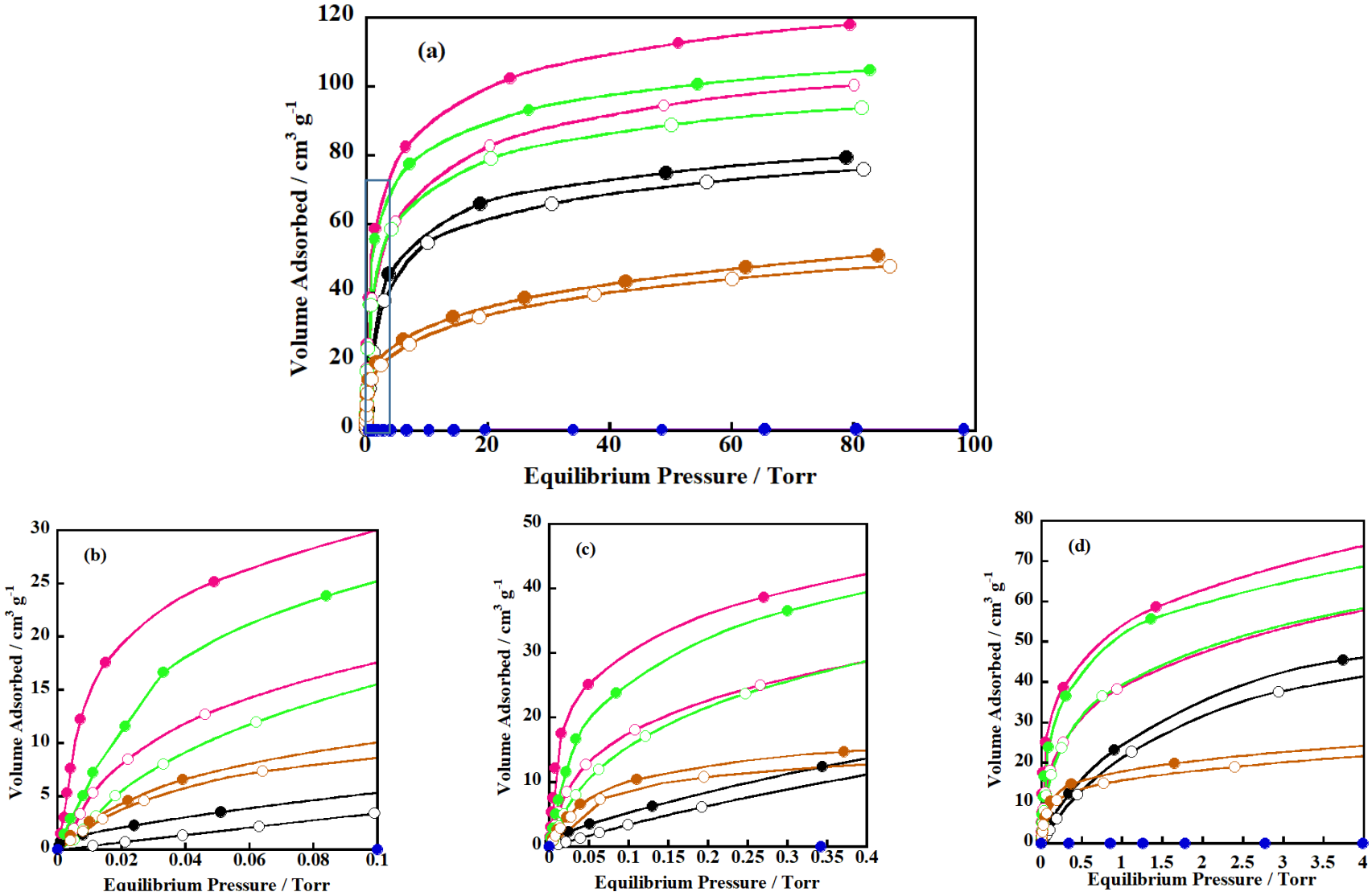


Figure 1. Adsorption isotherms of $CO_2$ at 298 K on alkaline-earth ion-exchanged NaA samples evacuated at 723 K. On these samples, the first and second isotherms were measured. Solid and open markes correspond to the first and second adsorption, respectively; (red) NaCaA-85: (green), NaSrA-71: (brown), NaMg-42: (blue), BaNaA stamples, respectively; (a) 0–100 Torr. Enlarged figures in the lower pressure region which is marked with square in (a) are depicted in three stages of pressures; (b) 0–0.1 Torr, (c) 0–0.4 Torr, and (d) 0–4 Torr. For comparison, the adsorption isotherms of $CO_2$ on NaA (starting material) are also indicated: (black), NaA sample.

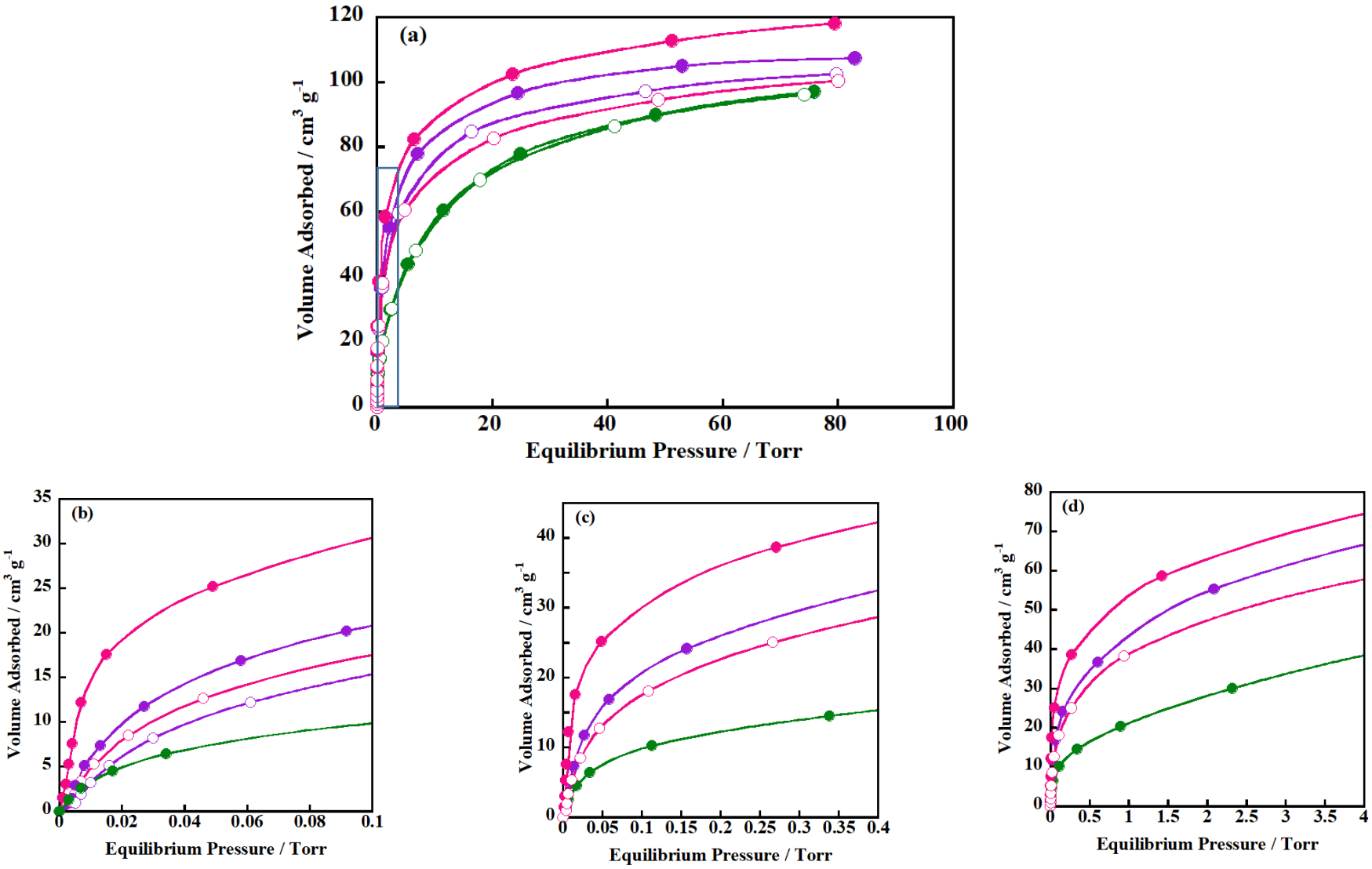


Figure 2. Adsorption isotherms of $CO_2$ measured at 298 K on alkaline-earth ion-exchanged NaA samples evacuated at 723 K. On these samples, the first and second isotherms were measured. Solid and open marks correspond to the first and second adsorption, respectively; (red) NaCaA-85: (violet), NaCaA-65: (green), CaA-78, respectively; (a) 0–100 Torr. Enlarged figures in the lower pressure region which is marked with square in (a) are depicted in three stages of pressures; (b) 0–0.1 Torr, (c) 0–0.4 Torr, and (d) 0–4 Torr.

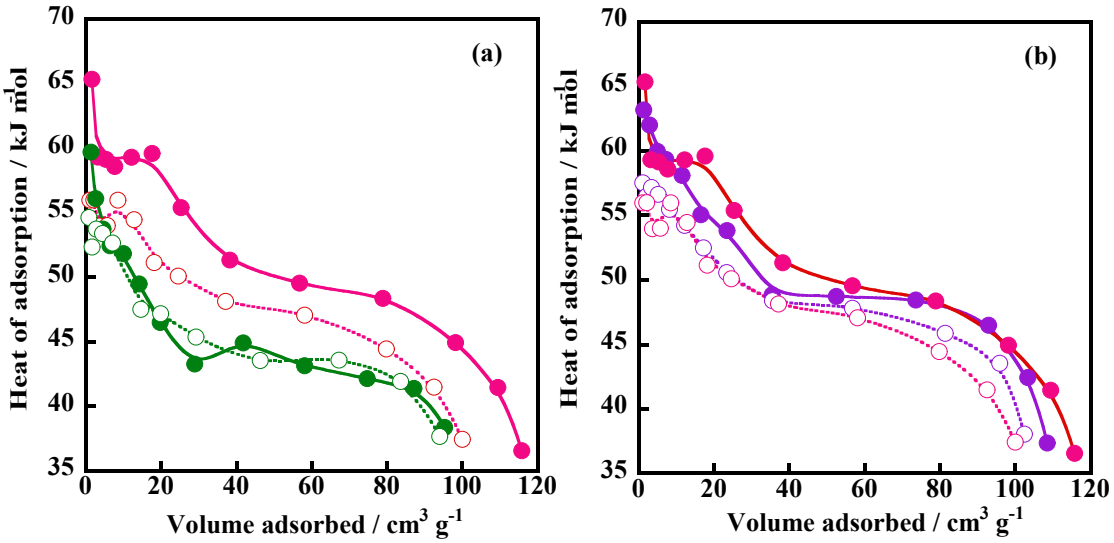


**Figure 3.** Differential heats of adsorption of $CO_2$ measured at 298 K on the NaCaA-85 (red), CaA-78 (green), and NaCa-65 (violet) samples. (a) Comparison between NaCaA-85 and CaA-78 samples, (b) Comparison between NaCaA-85 and NaCaA-65 samples. Solid and open marks represent the first (solid lines) and second (dotted line) adsorption processes, respectively.

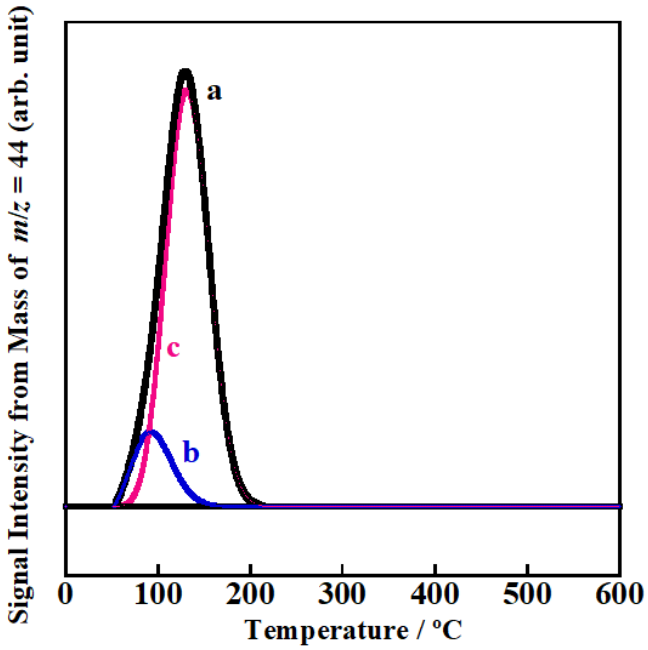


**Figure 4.** TPD of $CO_2$ adsorbed on the NaCaA-85 sample. First, the sample was evacuated at 723 K, followed by $CO_2$ adsorption around an equilibrium pressure of 100 Torr at RT, followed by evacuating at RT. After these treatments, the TPD measurement was performed. a: the curve observed in the evacuation process of this sample. This curve was deconvoluted into two components: curves b (weakly irreversibly-adsorbed species) and c (strongly irreversibly-adsorbed species), respectively.

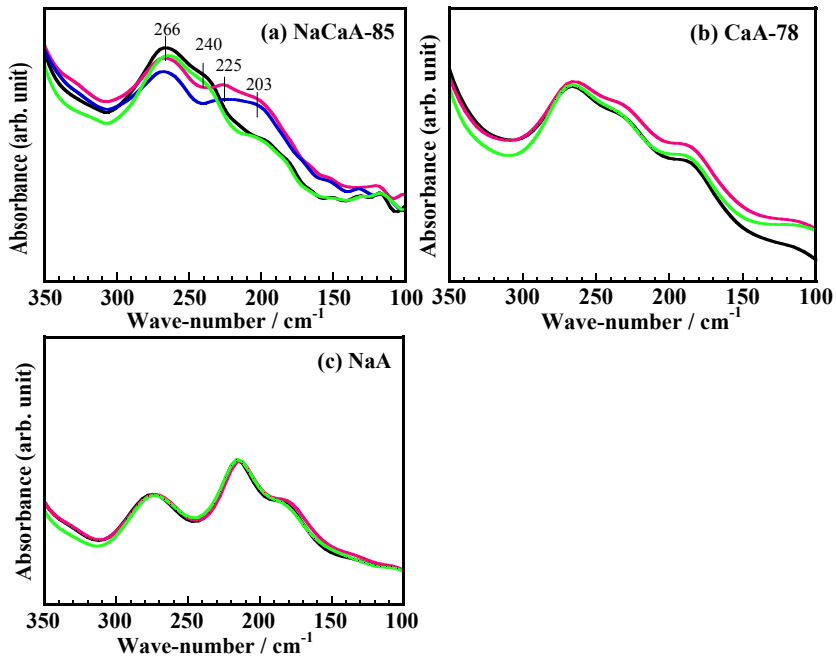


**Figure 5.** Changes in far-IR spectra before and after $CO_2$ adsorption at RT, and successive evacuation processes at 300 and 423 K. All measurements were carried out at RT. First, all samples were evacuated at 723 K as a standard treatment (black line), followed by equilibrating with $CO_2$ at RT (red line), re-evacuation at RT (blue line), and final re-evacuation at 423 K (green line). The series of treatments was performed *in situ*. (a) NaCaA-85, (b) CaA-78 and (c) NaA samples.

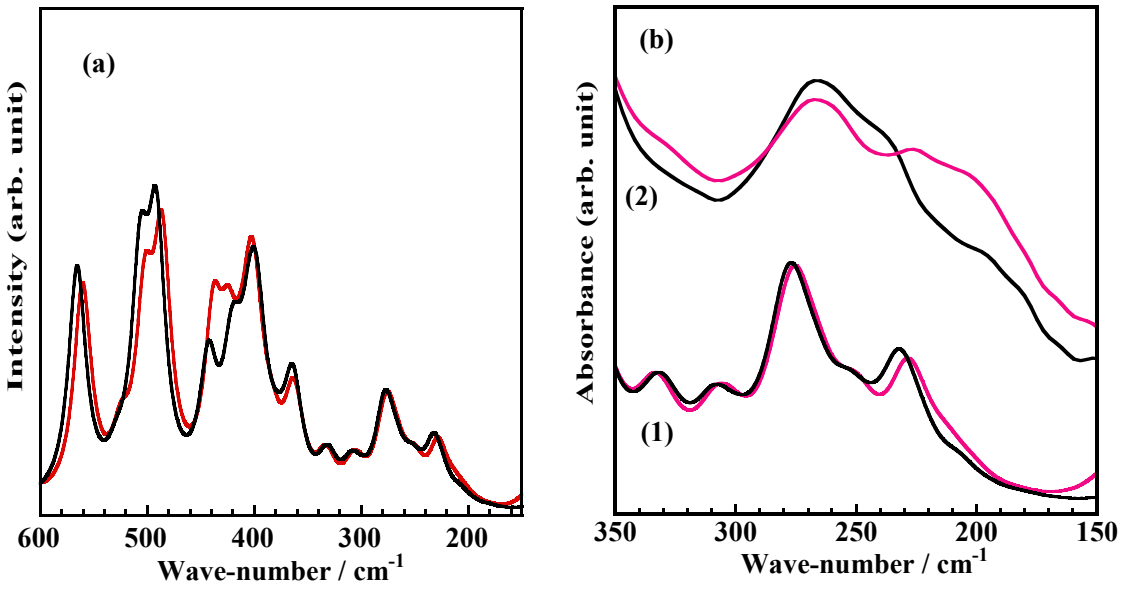


**Figure 6.** The results derived from the DFT calculation based on our proposed model in the far-IR region; the $CO_2$ molecule is simultaneously pinned by the $Ca^{2+}$ ions on two types of ion-exchanged sites composed of both the 6- and 8-MRs. (a) from 600 to 150 $cm^{-1}$ and (b) magnifying in the range between 350 and 150 $cm^{-1}$. In both figures, the **black** and **red** lines indicate before and after $CO_2$ adsorption, respectively. For comparison, the experimental results are also given in Figure 6b-(2) as spectra obtained before (evacuated at 723 K: **black** line) and after $CO_2$ adsorption at RT (**red** line), which are the same spectra given in Figure 5a. Both spectra were measured at RT.

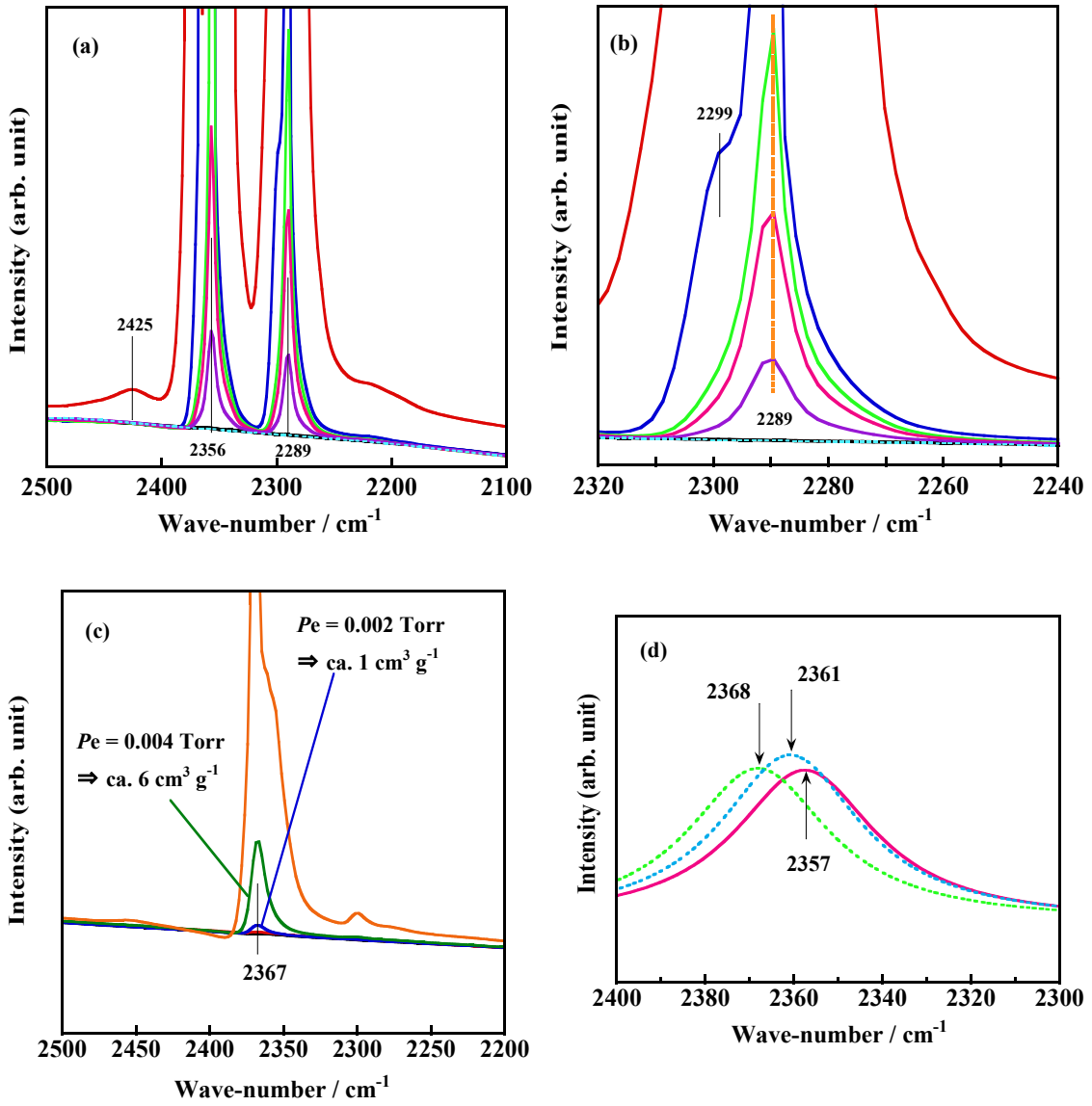


**Figure 7.** The mid-IR spectra of a mixture of gases composed of both $^{12}CO_2$ and $^{13}CO_2$ with the ratio of *ca*. 1:1 adsorbed on the NaCaA-85 sample at RT: (a) between 2500 and 2100 $cm^{-1}$ and (b) magnified in the range between 2320 and 2240 $cm^{-1}$. All measurements were performed at RT: (**black**) evacuated at 723 K, (**brown**) exposed to mixed isotope gas of $CO_2$ under the equilibrium pressure of 1.84 Torr, and successively evacuated at RT, (**blue**): at 323 K, (**green**): at 348 K, (**red**): at 373 K, (**violet**): at 423 K (**light blue dotted line**), respectively.
(c) $^{12}CO_2$ was adsorbed at RT on the NaCaA-85 sample evacuated at 723 K (**black**), and successively equilibrated with considerably lower pressures: 0.001 Torr, (**red**): 0.002 Torr, (**blue**): 0.004 Torr, (**green**): 0.014 Torr, **(brown)**, respectively.
(d) Results from the DFT calculation based on three kinds of models in the mid-IR region; (**red**), the $CO_2$ molecule is simultaneously pinned by the $Ca^{2+}$ ions on two types of ion-exchanged sites composed of both 6- and 8-MRs: (**dotted light blue**), adsorbed on the 6-MR: **(dotted green line)**, adsorbed on the $Ca^{2+}$ ion exchanged on the 8-MR.

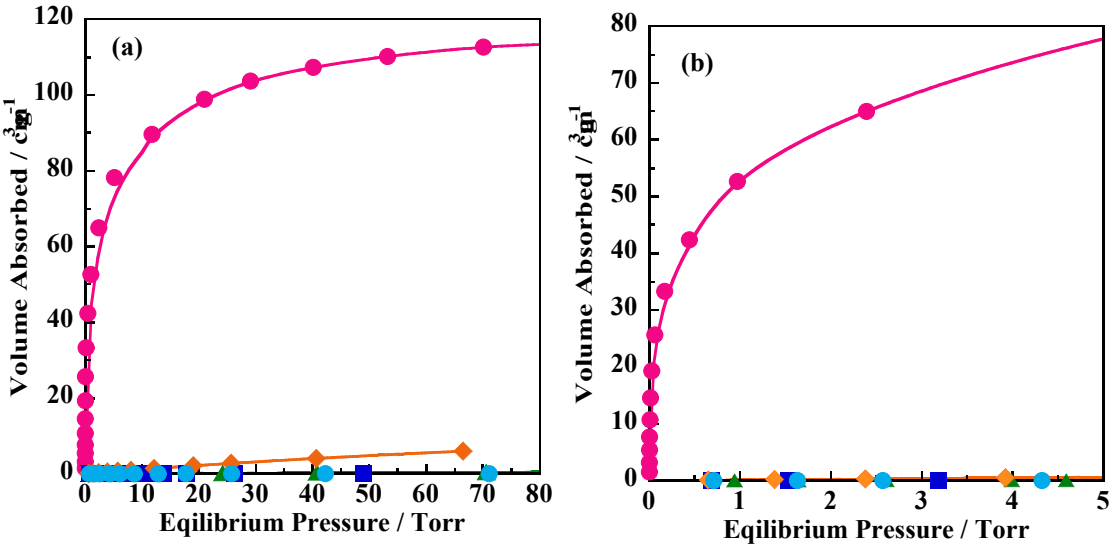


**Figure 8.** Adsorption isotherms of various gases on the NaCaA-85 sample evacuated at 723 K. All measurements were performed at 298 K. Equilibrium pressure; (a) from 0 to *ca*. 80 Torr and (b) magnified in the range between 0 and 5 Torr; (**green triangle**), $N_2$: (**red solid circle**), $CO_2$: (**blue square**), $O_2$: (**brown diamond**), $CH_4$: (**light blue circle**), $H_2$.

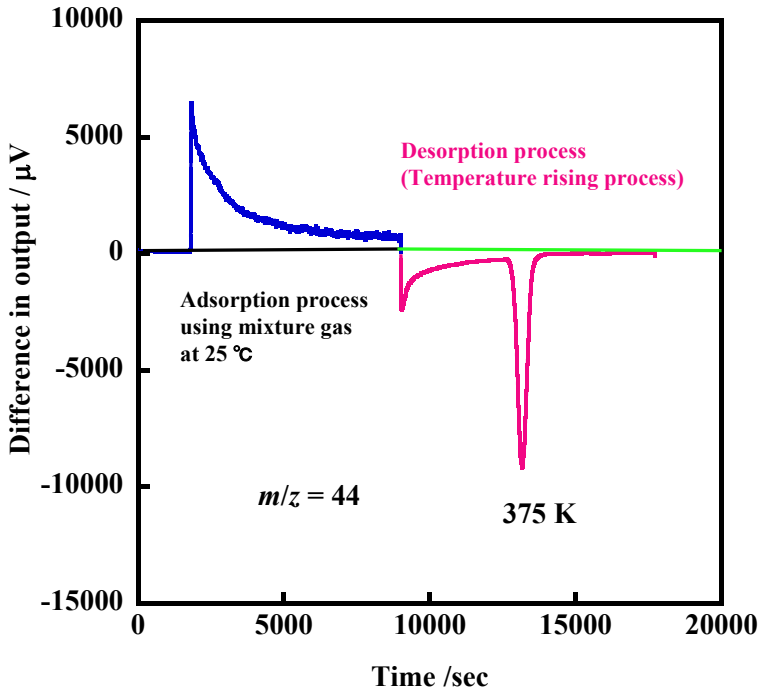


**Figure 9.** Breakthrough curve of $CO_2$ adsorption and desorption measured by use of a gas mixture mimicking the atmospheric components composed of $CO_2$, $O_2$ and $N_2$ (0.04%, 20%, and 79.96%, respectively). The first process corresponds to the change in $CO_2$ pressure (adsorption) and the second to desorption of adsorbed $CO_2$. The latter process was composed of two parts; desorption caused by the weakly irreversibly-adsorbed and strongly irreversibly-adsorbed species, respectively.